

Subkilometer Simulation of a Torrential-Rain-Producing Mesoscale Convective System in East China. Part I: Model Verification and Convective Organization

MAN ZHANG

Key Laboratory of Meteorological Disaster and College of Atmospheric Sciences, Nanjing University of Information Science and Technology, Nanjing, China, and Department of Atmospheric and Oceanic Science, University of Maryland, College Park, College Park, Maryland, and Cooperative Institute for Research in the Atmosphere, Colorado State University, Fort Collins, Colorado

DA-LIN ZHANG

Department of Atmospheric and Oceanic Science, University of Maryland, College Park, College Park, Maryland

(Manuscript received 25 January 2011, in final form 26 June 2011)

ABSTRACT

A nocturnal torrential-rain-producing mesoscale convective system (MCS) occurring during the mei-yu season of July 2003 in east China is studied using conventional observations, surface mesoanalysis, satellite and radar data, and a 24-h multinested model simulation with the finest grid spacing of 444 m. Observational analyses reveal the presence of several larger-scale conditions that were favorable for the development of the MCS, including mei-yu frontal lifting, moderate cold advection aloft and a moist monsoonal flow below, and an elongated old cold dome left behind by a previously dissipated MCS.

Results show that the model could reproduce the evolution of the dissipating MCS and its associated cold outflows, the triggering of three separate convective storms over the remnant cold dome and the subsequent organization into a large MCS, and the convective generation of an intense surface meso-high and meso- β -scale radar reflectivity morphologies. In particular, the model reproduces the passage of several heavy-rain-producing convective bands at the leading convective line and the trailing stratiform region, leading to the torrential rainfall at nearly the right location. However, many of the above features are poorly simulated or missed when the finest model grid uses either 1.33- or 4-km grid spacing. Results indicate the important roles of isentropic lifting of moist monsoonal air over the cold dome in triggering deep convection, a low-level jet within an elevated moist layer in maintaining conditional instability, and the repeated formation and movement of convective cells along the same path in producing the torrential rainfall.

1. Introduction

The mei-yu front, occurring during the months of May–July in East Asia, is the northernmost boundary of moist monsoon air originating from the southwest at which large-scale atmospheric conditions become favorable for deep convection and extensive stratiform precipitation. Unlike the typical midlatitude counterpart elsewhere, the mei-yu front is characterized by weak temperature gradients but high equivalent potential temperature θ_e gradients (due to strong moisture contrast) and large horizontal

wind shear (Ding and Chan 2005). In general, the mei-yu front accounts for a sizeable amount of annual rainfall over the Yangtze-Huai River Basin (YHRB), that is located between the Yangtze River and Huai River (roughly within the belt of 30°–33°N, see Fig. 1 for the location) in east China (Ding and Chan 2005). Because of its quasi-stationary nature, flash flooding often occurs in the YHRB when intense convective cells move repeatedly over the same area along the front, a process called “echo training” by Doswell et al. (1996). This has attracted many observational and modeling studies to examine various aspects of the mei-yu frontal systems and their associated heavy rainfall (e.g., Chen and Yu 1988; Chen et al. 1998; Qian et al. 2004). However, most of the previous studies focused on the large-scale moisture supply by monsoonal flows, prestorm environments, local precipitation recycling,

Corresponding author address: Dr. Da-Lin Zhang, Department of Atmospheric and Oceanic Science, University of Maryland, College Park, College Park, MD 20742-2425.
E-mail: dalin@atmos.umd.edu

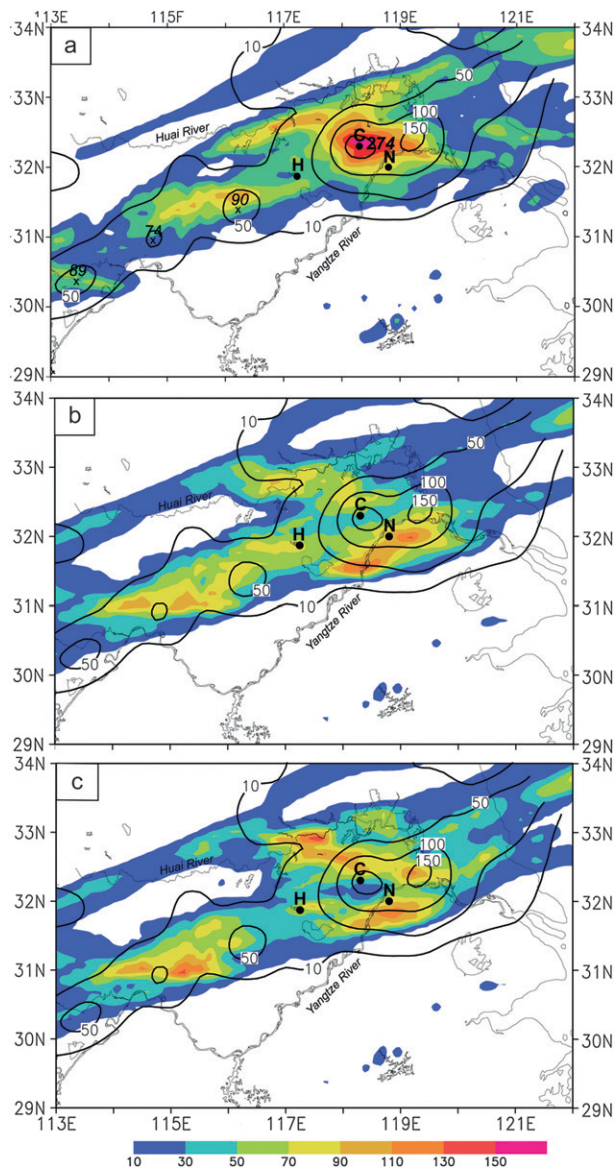


FIG. 1. (a) Comparison of the 24-h accumulated rainfall (mm) between the control-simulated (shaded) and the rain gauge observed (contoured) ending 0000 UTC 5 Jul 2003. (b) As in (a), but for the nested 12/4/1.33-km run. (c) As in (a), but for the nested 12/4-km run. Letters “C,” “N,” and “H” denote the cities of Chuzhou, Nanjing, and Hefei, respectively; and the Yangtze River and Huai River are also indicated. (This is the same for the rest of the figures.)

low-level jets (LLJs), the impact of mesoscale convective systems (MCSs) or mesovortices along the mei-yu front, and cloud-precipitation morphology as seen from satellite and radar data [see Ding and Chan (2005) for a review]; similarly for numerous observational studies of heavy-rainfall events occurring in the United States (e.g., Maddox et al. 1979; Caracena et al. 1979; Bosart and Sanders 1981; Schumacher and Johnson 2005, 2009).

Despite the numerous studies in the past decades, our ability to predict and understand torrential rainfall (associated with the mei-yu front) and quantitative precipitation forecasts (QPFs) in general is very limited because of the lack of high-resolution observations and deficiencies in numerical weather prediction (NWP) models (Fritsch et al. 1998). After all, heavy rainfall is an end product of multiscale nonlinear interactions ranging from cloud microphysical processes to cloud dynamics, MCSs, the mei-yu front, and the East Asian monsoon. Although several related field experiments have been conducted in East Asia (e.g., the Taiwan Area Mesoscale Experiment in 1987 and the YHRB experiments in 1998 and 2008) and elsewhere during the past several decades, they could only provide snapshots of MCSs (and mei-yu systems) at certain stages of their life cycles. In particular, changes in rainfall intensity and locations of rainfall maxima are more challenging to estimate, because they are closely associated with the unsteady evolution of convective cells and their nonlinear interactions with moist environments. Moreover, these small-scale features could not be resolved by the current operational NWP models, and they are also difficult to observe even with today’s state-of-the-art observing systems because high-resolution data must be obtained in the heavy-rainfall-producing portion of an MCS, where rapid structural changes take place. All of these make high-resolution numerical modeling a viable option for studying the multiscale interactions involved in heavy-rain-producing MCSs along the mei-yu front.

With the rapid growth of computing power in recent years, we have begun seeing real-data cloud-resolving simulations of MCSs and even cloud-resolving NWP at some operational centers with the grid sizes of 1–4 km, in contrast to much coarser-resolution (>20 km) simulations with convection parameterized, conducted 25 years ago (e.g., Zhang and Fritsch 1986). Previous modeling studies showed that coarse-resolution models tend to produce excessive rainfall, mostly associated with grid-scale condensation as a result of a (conditional instability of the second kind) CISK-like mechanism, when parameterized convection fails to remove conditional instability (Zhang et al. 1988; Molinari and Dudek 1992; Zhang et al. 1994). Recently, Clark et al. (2009) compared precipitation forecast skill between a 5-member, 4-km-resolution cloud-resolving ensemble and a 15-member, 20-km-resolution convection-parameterized ensemble for 23 warm-season cases that occurred over the central United States, and found more accurate rainfall forecasts with the cloud-resolving ensemble. Similarly, Weisman et al. (2008) showed significant improvements of the 4-km cloud-resolving real-time forecasts in representing MCS modes (i.e., squall lines, bow echoes,

mesovortices) and the diurnal convective cycle during three growing seasons of 2003–05, as compared to the 12-km operational NWP with parameterized convection. Based on these results, it appears to be desirable to use high-resolution cloud-resolving models to predict summertime rainfall.

Indeed, after systematically examining the NWP of convective rainfall events that occurred in the United Kingdom during the summer seasons of 2003–05 using the Met Office Unified Model with the 1-, 4- and 12-km grid spacing, respectively, Lean et al. (2008) found that the finer grid models tend to produce more realistic rainfall structures and verification scores, with less delay in convective initiation than coarser resolution models, although some finescale features are poorly represented during the first few integration hours when they are spun up from the coarser-resolution fields. On the other hand, some recent studies indicated that while decreasing grid spacing from 4 to 2 km shows more realistic convective and rainfall structures, it provides little added value as next-day guidance for predicting the occurrence of MCSs and heavy rainfall (e.g., Kain et al. 2008; Weisman et al. 2008; Schwartz et al. 2009). These different modeling results appear to depend not only on grid spacing, but also on the larger-scale environments in which MCSs developed, the quality of the model initial conditions, and the realism of model physics representations.

Cloud-resolving models with the finest 2–4-km grid spacing have also been used to simulate and study the finescale circulations and multiscale-interactive processes leading to the development of heavy-rainfall events. For instance, Kato and Goda (2001) examined the formation and maintenance processes associated with a heavy-rain-producing convective band. Kato (2006) showed a hierarchy of cloud structures with different horizontal scales that developed successively upstream and moved through the same location along a cold front, leading to the realistic generation of heavy rainfall. Trier et al. (2006) investigated statistically the mechanisms supporting the long-lived episodes of zonally propagating heavy-rainfall events occurring over the central United States, including the continuous generation of deep convection along cold outflow boundaries, the roles of the LLJs in organizing nocturnal MCSs and enhancing frontogenesis, and the associated vertical circulations.

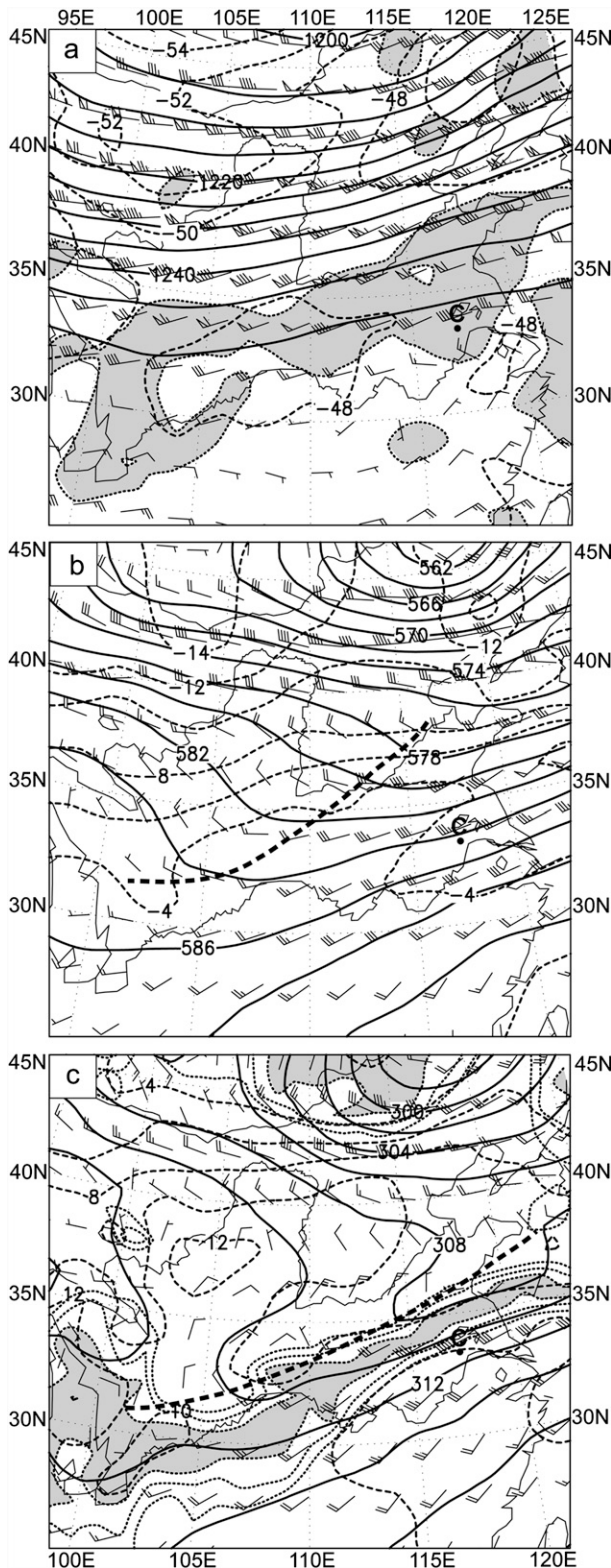
While the rapid growth in computing power has allowed us to use the 1-km grid spacing to simulate MCSs (e.g., Lean et al. 2008), Bryan et al. (2003) found that such a grid spacing still could not produce many convective structures and evolution of squall lines in numerical simulations. Their idealized modeling work suggests the necessity to use an NWP model with grid spacing of order 100 m to resolve the inertial subrange in turbulent

kinetic energy spectrum. Clearly, a grid spacing of 2–4 km, used by most of the previous studies, could only resolve large, organized cumulonimbi (e.g., with a filtered scale of greater than 12 km), because convective overturning always tends to occur at the smallest resolvable scale. In particular, many localized convective cores, linear rainbands, moist downdrafts and vortices, and extreme rainfall events are too small to be adequately resolved (Zhang et al. 2009), and their intensities are also very sensitive to grid resolution. Furthermore, none of the above-mentioned studies has examined the triggering of deep convection, heavy-rainfall structures, and convectively generated meso- β -scale circulations.

During the evening hours of 4 July 2003, a torrential-rain-producing MCS developed ahead of a mei-yu front over the YHRB, producing about 274 mm of rain at Chuzhou, China, in the 24-h period ending at 0000 UTC 5 July. This MCS was intensively observed during a field experiment studying the mei-yu heavy rainfall, and covered by several radars in the cities of Hefei (H) and Nanjing (N), China, that are about 100 and 50 km to the southwest and southeast of Chuzhou, respectively (see Fig. 1 for their locations). Because of the additional field observations, this case has attracted several observational and (coarse resolution) modeling studies to examine the larger-scale conditions for the development of and the radar reflectivity structures of the MCS (Sun et al. 2006), and the generation of heavy rainfall along the mei-yu front (Liao and Tan 2005; Wang and Ni 2006) as well as the predictability of the MCS (M. Zhang et al. 2006).

This study is the first in a series of papers that address the aforementioned issues through a numerical investigation of multiscale interactions involved in the heavy-rainfall event. The objectives of the present study are to (i) document the large- and mesoscale conditions that were favorable for the generation of torrential rainfall associated with the MCS; (ii) explore the multiscale processes associated with the triggering and organization of deep convection leading to the torrential rainfall; and (iii) investigate the general implications for subkilometer simulations of MCSs and the potential improvements of QPFs and the pertinent mesoscale circulations, as verified against available observations. They will be achieved using multiscale observational analyses and a 24-h multiscale simulation of the 4–5 July 2003 MCS and its associated torrential rainfall in Chuzhou with the finest subkilometer grid spacing.

The next section provides an overview of the synoptic-scale forcing, surface mesoscale circulations, and the observed torrential-rainfall events. Section 3 describes the model configuration, including the model initial conditions. Section 4 shows verification of the model-simulated



mesoscale features against rain gauge, satellite, and radar observations. Section 5 examines the triggering and organization of deep convection, as well as meso- β -scale surface features associated with the heavy-rain-producing MCS. A summary and conclusions are given in the final section.

2. Overview

The torrential-rainfall event of interest occurred during the evening hours of 4 July 2003 as a new MCS developed behind a dissipated MCS on the (southern) moist side of the mei-yu front over the YHRB (Fig. 1). Of relevance to this study is that this case took place during an intense observing period of a mesoscale field experiment studying heavy-rain-producing MCSs along the mei-yu front. Thus, the associated additional upper-air rawinsondes and some radar observations about the MCS will be useful for the present study.

Figure 1a shows the distribution of 24-h accumulated rainfall (contoured, in mm) ending at 0000 UTC 5 July 2003 exhibiting a southwest–northeast-oriented rainfall belt with a width of 120–160 km and a length of over 1000 km over the YHRB. There are four rainfall centers, with the heaviest amount of 274 mm recorded near the city of Chuzhou, denoted by the letter “C” in all figures. A meso- β area of about $150 \text{ km} \times 80 \text{ km}$ in (x, y) in the vicinity of Chuzhou received more than 100 mm. Note that most of this rainfall was observed during the evening hours, with more than half occurring during the 6-h period from 1200 to 1800 UTC 4 July. The generation of the associated extreme rainfall events is of primary concern in this study.

Figure 2 shows the National Centers for Environmental Prediction (NCEP) $1^\circ \times 1^\circ$ Final (FNL) Analysis at 0000 UTC (or 0800 LST) 4 July 2003, that was about 12 h prior to the initiation of the MCS of interest. The 200-hPa map shows a South Asian anticyclone over the Tibetan Plateau in southeastern China, with an upper-level jet stream of over 65 m s^{-1} and a warm anomaly in the stratosphere to the north. The YHRB was just located within an elongated divergent zone (shaded) in the westerly flow branch of the anticyclone, which coincided

FIG. 2. Horizontal distribution of geopotential height (solid), temperature (dashed), and wind barbs from the NCEP FNL analysis at 0000 UTC 4 Jul 2003 at (a) 200 hPa with the horizontal divergence exceeding 10^{-5} s^{-1} shaded, (b) 500 hPa, and (c) 700 hPa with the relative humidity (dotted, every 10% from 70%) exceeding 90% shaded. Thick dashed lines in (b) and (c) denote the trough axis. A full barb is 5 m s^{-1} .

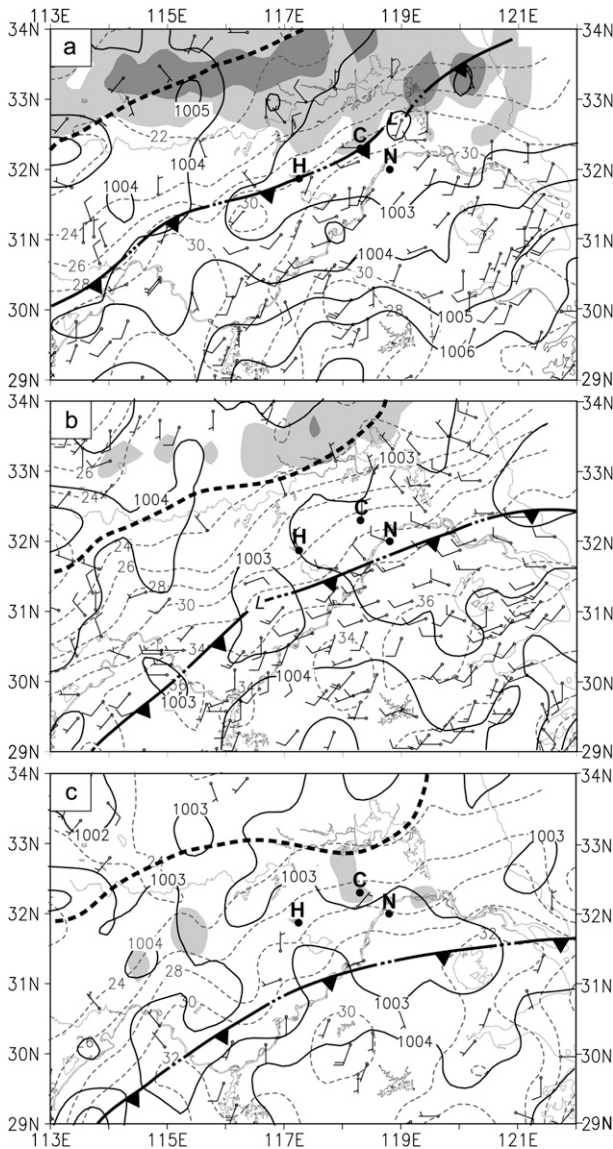


FIG. 3. Surface observational analysis of the sea level pressure (solid, every 1 hPa), surface temperature (dashed, every 2°C), and surface winds, superimposed with the accumulated rainfall (10-mm light shaded, and greater than 50-mm dark shaded) during the 6-h period ending at (a) 0000, (b) 0600, and (c) 1200 UTC 4 Jul 2003. Thick dashed lines denote the distribution of $\theta_e = 345$ K or the mei-yu front at 850 hPa. Cold and warm frontal symbols alternated with double dots indicate moist-downdraft outflow boundaries (this is the same for the rest of the figures). A full barb is 5 m s^{-1} , and only surface wind speeds greater than 2.5 m s^{-1} are shown.

with the distribution of a mei-yu front (cf. Figs. 2a,c and 3a). This organized divergence zone appears to be closely related to an elongated southwest–northeast-oriented MCS, that was active during the previous evening hours (cf. Figs. 2a, 3a, and 4). At 500 hPa, a mobile trough with significant cold advection behind its axis approaches the YHRB from the northwest. Of

importance is that the thermal advection in that region is only a midlevel phenomenon, as can be corroborated by comparing Fig. 2b with Figs. 2a,c. This suggests that the larger-scale environment ahead of the mei-yu front tended to become gravitationally destabilized with time. The pronounced horizontal wind shear, weak thermal gradients but large moisture contrast across a typical mei-yu front could be clearly seen from the 700-hPa map (Fig. 2c). For the sake of clarity, we define herein the mei-yu front as roughly corresponding to the $\theta_e = 345$ -K surfaces (see thick dashed lines in Figs. 3–5, and the remaining figures). Then, we see that the mei-yu front was located ahead of the shear line–trough axis and slightly behind an elongated high humidity zone. This indicates that the tropical high- θ_e air could not be lifted during its northward course under the influence of the subtropical high until it met with the mei-yu front.

The corresponding mesoscale surface analyses are given in Fig. 3, which shows an elongated cold dome with a minimum temperature of 22°C ahead of the mei-yu front, and outflows toward its warmer sides. This cold dome was about 8°C colder than the surface air to the south at this early morning hour (i.e., 0000 UTC 4 July), and it was generated by the dissipating MCS that was initiated 12 h earlier (not shown). This MCS produced considerable amount of rainfall ahead of the mei-yu front during the previous evening hours; some regions received more than 50 mm during the past 6 h. However, this storm began to dissipate in conjunction with the weakening of the LLJ as it moved southeastward into East China Sea by 1500 UTC 4 July (cf. Figs. 4c and 5). As will be shown from the model simulation, the cold dome left behind played an important role in triggering new convection, assisting in the formation of the extreme rain-producing MCS when more convective available potential energy (CAPE) could be supplied. It should be mentioned that none of the previously mentioned studies of the case has examined the impact of the cold dome on the subsequent development of the MCS.

In fact, the southwesterly winds transported continuously tropical high- θ_e air from South China Sea into the region ahead of the mei-yu front. This could be seen from the vertical cross section of thermodynamic variables in Fig. 5, showing the presence of high- θ_e (greater than 355 K) air in the planetary boundary layer (PBL) and low- θ_e air (less than 330 K) near 600 hPa with marked potential instability in the deep southwesterly flows. Figure 5 also shows that (i) a weak cold dome behind the mei-yu front was meridionally sandwiched by warm air masses below 800 hPa, and (ii) the $\theta_e = 345$ -K contour, that roughly represents the mei-yu frontal surface, delineates well the northern edge of the southwesterly monsoonal air with high humidity columns associated with the dissipating

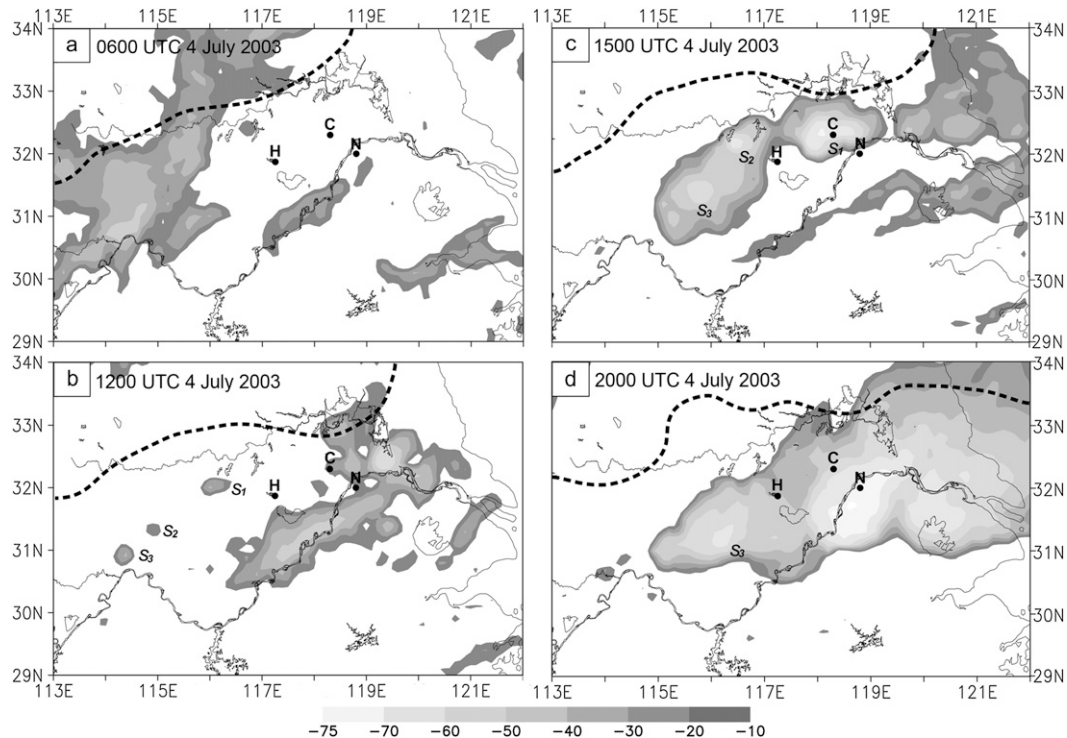


FIG. 4. Time evolution of the cloud-top blackbody temperature (TBB) of less than -10°C derived from China's FY-geostationary satellite at (a) 0600, (b) 1200, (c) 1500, and (d) 2000 UTC 4 Jul. Thick dashed lines denote the distribution of $\theta_e = 345\text{ K}$ or the mei-yu front at 850 hPa. Symbols "S₁," "S₂," and "S₃" are used to trace the initiation of three convective storms.

MCS. It appears that the NCEP FNL analysis underestimates the intensity of the cold pool because it did not assimilate the dense surface observations. Note the upper-level cold air anomaly behind the front that was closely related to an extratropical cyclone to the north (cf. Figs. 5 and 2b), but less relevant to the convective developments in the YHRB.

Six hours later (i.e., at 0600 UTC 4 July), the cold dome still kept its intensity and structures likely due to the continued evaporative cooling and cloud-shading effects from the dissipating storm (Figs. 3b and 4a). (Note that although the dissipating MCS passed by Chuzhou, it did not drop much precipitation over the region.) In contrast, the surface air under the clear sky had been warmed up by 4° – 6°C , thereby increasing the surface temperature gradients on both sides of the front. Despite the favorable larger-scale environment and the pronounced low-level baroclinic forcing, new convection did not develop until the early evening (i.e., 1200 UTC 4 July) when the surface cold outflow boundaries became loosely organized (Fig. 3c).

Cloud-top blackbody temperature (TBB) data, in the range (-10°C , -75°C) at this time shows the initiation of three isolated convective elements (i.e., S₁, S₂, and S₃ in Fig. 4) along a line in the wake of the dissipating MCS;

they were located about 100 km ahead of the mei-yu front, but far behind the leading cold outflow boundaries. The convective element S₁ arrived near Chuzhou 3 h later (Fig. 4c), dropping considerable rainfall along its track. The convective elements expanded rapidly in coverage as they moved northeastward along the quasi-stationary mei-yu front, and by 2000 UTC 4 July, they were merged to form a new MCS with more extensive stratiform clouds downstream (Figs. 4c,d). The movement of the cold cloud tops coincided well with the generation of heavy rainfall to the southwest of Hefei, and at Chuzhou and Nanjing (cf. Figs. 1 and 4). This MCS caught up and then merged with the dissipating MCS ahead, and moved away from the region of interest by 0000 UTC 5 July (not shown).

3. Model description

In this study, the multiscale processes leading to the development of torrential rainfall over the YHRB are explicitly simulated using a two-way interactive, quadruply nested (12/4/1.33/0.444 km) grid (Zhang et al. 1986), cloud-resolving version of the fifth-generation Pennsylvania State University–National Center for Atmospheric Research

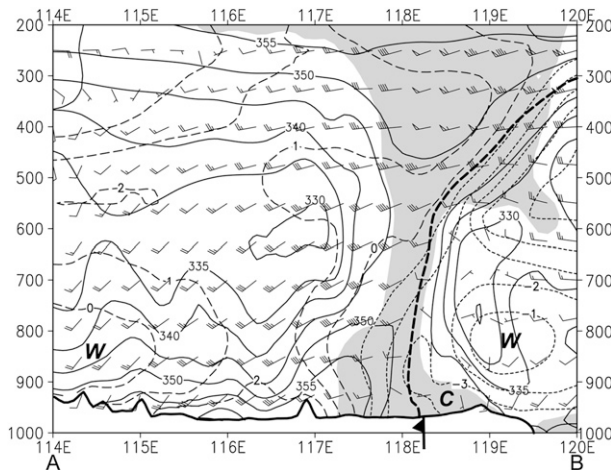


FIG. 5. Vertical cross section of the equivalent potential temperature (θ_e , every 5 K), deviation temperature (positive–dashed and negative–dotted, every 1°C), superimposed with horizontal wind barbs (a full barb is 5 m s^{-1}), which is taken from the NCEP FNL analysis at 0000 UTC 4 Jul 2003, along line AB given in Fig. 6. Deviation temperature is obtained by subtracting the mean temperature at each level in the cross section. Relative humidity exceeding 90% is shaded. The location of the surface outflow boundary and topography is plotted. Thick dashed lines denote the distribution of $\theta_e = 345 \text{ K}$ or the mei-yu front.

(PSU–NCAR) Mesoscale Model (i.e., MM5, version 3.6). The model physical processes include (i) the simultaneous use of the updated Kain–Fritsch (Kain 2004) cumulus parameterization and the Tao and Simpson (1993) three-ice cloud microphysics scheme for the 12- and 4-km grid meshes, *but only the latter is used for the 1.33- and 0.444-km meshes*; (ii) a modified version of the Blackadar PBL parameterization (Zhang and Anthes 1982); and (iii) a cloud–radiation interaction scheme (Dudhia 1989). The land surface temperature is predicted using the surface energy budget equation, in which the effects of short- and longwave radiation and cloud radiation are included. For a more detailed description of MM5, the reader is referred to Dudhia (1993) and Grell et al. (1995).

Figure 6 shows the four nested model domains with Lambert map projection, which have the (x, y) dimensions of 202×232 (D1), 385×391 (D2), 385×391 (D3), and 385×391 (D4) with the grid sizes of 12, 4, 1.33, and 0.444 km, respectively. Note that this 444-km grid spacing is about 200 m larger than that suggested by Bryan et al. (2003) to resolve an inertial subrange. A large domain size of the outermost mesh (i.e., D1) with the western boundary set at the foothill of the Tibetan Plateau is used in order to minimize the influence of the lateral boundary conditions on the evolution of MCSs of interest. The intermediate 4- and 1.33-km resolution meshes (i.e., D2 and D3) are used to simulate the mesoscale and storm-scale flows, and cover the initial slow and the subsequent

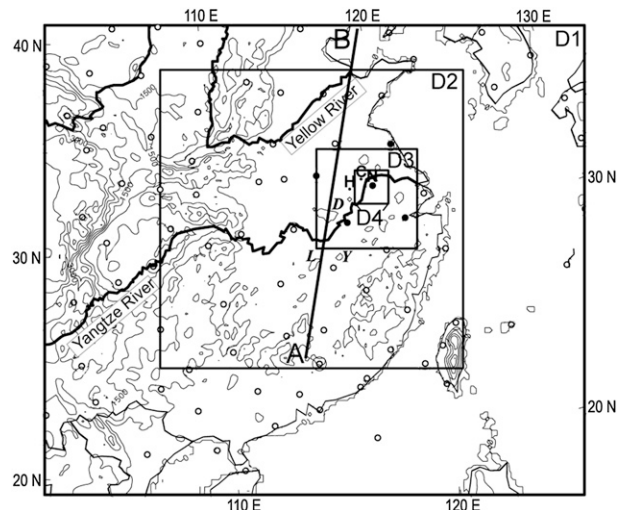


FIG. 6. Model domains (D1–D4), superposed with topography at intervals of 500 m and the distribution of conventional (open circles) and field-experimental (solid circles) rawinsonde stations as well as Yangtze River and Yellow River. Letters “D,” “L,” and “Y” indicate Mt. Dabie, Mt. Lu, and Mt. Yellow, respectively. Line A–B shows the location of vertical cross section shown in Fig. 5.

rapid intensification stages of the storm, respectively. The finest mesh (D4) with a grid size of 444 m is designed to resolve explicitly discrete convective cells, as shown in Zhang et al. (2009). A total of 40 uneven terrain-following σ -coordinate levels¹ (for all the grid meshes) with higher resolution in the PBL are used in the vertical. The model top is set at 30 hPa.

The model is initialized at 0000 UTC (i.e., 0800 LST) 4 July 2003 using the NCEP FNL $1^\circ \times 1^\circ$ analysis, which is then enhanced by conventional observations (open circles in Fig. 6) and 5 additional soundings taken during the field campaign (solid circles in Fig. 6), using the standard objective analysis tools in the MM5 modeling system. It is apparent from Fig. 6 that the high-resolution (about 250–350 km) observations upstream play an important role in determining the quality of the present case simulation. To produce as realistically as possible the model initial conditions and the outermost lateral boundary conditions, we first improve the NCEP FNL analysis at 6-h intervals by enhancing it with the conventional and field observations. Then, a 36-h single-domain dynamic-nudging integration (Stauffer and Seaman 1990), initialized 12 h earlier (i.e., at 1200 UTC 3 July) with the enhanced analysis and targeted toward the enhanced 6-hourly analyses, is performed with a grid size of 36 km over a domain much

¹ The 40 σ -coordinate levels are 1.0, 0.999, 0.9975, 0.995, 0.9925, 0.99, 0.985, 0.98, 0.97, 0.96, 0.95, 0.94, 0.93, 0.92, 0.91, 0.9, 0.88, 0.86, 0.84, 0.82, 0.8, 0.77, 0.74, 0.7, 0.65, 0.6, 0.55, 0.5, 0.45, 0.4, 0.35, 0.3, 0.25, 0.2, 0.15, 0.1, 0.075, 0.05, 0.025, and 0.

TABLE 1. The model design.

Domain	D1	D2	D3	D4
Dimensions (x, y)	202 \times 232	385 \times 391	385 \times 391	385 \times 391
Area coverage (km ²)	2412 \times 2772	1536 \times 1560	512 \times 520	171 \times 173
Grid size (km)	12	4	1.33	0.444
Time step (s)	36	12	4	1.33
Integration hours	0–24	6–24	12–24	12–24

larger than D1 (not shown). The 12-h nudging simulation output fields are interpolated to the (D1) 12-km resolution mesh as the model initial conditions, and the 6-hourly output fields from 12–36-h nudging simulations are used to specify the outermost lateral boundary conditions. Note that the model initial time is about 12 h prior to the formation of the MCS under study (Fig. 4). To minimize computational costs, D2 is activated at 6 h into the integration, and the cloud-resolving domains D3 and D4 are activated at 12 h into the integration. The initial conditions over each finer-mesh domain are always interpolated from the coarser mesh data during the model integration. A 24-h model integration is conducted, ending at 0000 UTC 5 July, which is just long enough to cover the life cycle of the MCS of interest, including the generation of its associated torrential-rainfall events. See Table 1 for more details.

4. Model verification

In this section, we verify the 24-h simulation of the extreme rainfall events that occurred ahead of a mei-yu front against various observations (e.g., surface analyses, satellite and radar observations). More attention will be paid to ascertaining whether or not a subkilometer cloud-resolving simulation (i.e., during the second 12-h integration) could have any positive impact on the QPFs of the case, from convective triggering to rainfall intensity and distributions. This is not a trivial task since the model is initialized by the large-scale initial conditions, even with the inclusion of a few additional upper-air observations.

Figure 1a compares the 24-h accumulated rainfall over the YHRB to the amounts observed. It is encouraging that the nested-grid model reproduces quite well the general pattern and magnitude of the 24-h accumulated rainfall, including the three rainfall centers to the southwest. In particular, the model reproduces the extreme rainfall (shaded), with an amount of over 160 mm, near Chuzhou and a coverage of larger than 100 mm downstream over the Chuzhou–Nanjing area.

To show the importance of using the subkilometer grid spacing for the present study, we have rerun the case with the same model configurations as those described in section 3 except for the different finest grid spacings. The

24-h accumulated rainfall from the 12/4/1.33-km and 12/4-km nested-grid simulations are given in Figs. 1b and 1c and referred to as the 1.33- and 4-km runs, respectively, as compared to that from the 12/4/1.33/0.44-km control (CTL) run shown in Fig. 1a. Obviously, both sensitivity runs misplace considerably the location of the peak rainfall. Instead, several rainfall belts are simulated, with more localized rainfall occurring to the south of Nanjing and northwest of Chuzhou but little between them. The peak rainfall amounts in both runs are about 60% of the CTL-simulated. Moreover, a sizeable portion of the peak rainfall in the 4-km run is generated by grid-scale condensation (not shown). More significant contribution of the grid-scale precipitation occurs, causing numerical point storms, in the present case as the finest grid spacing increases further to 12 km (M. Zhang et al. 2006). Although Liao and Tan (2005), and Wang and Ni (2006) could simulate a heavy-rainfall center near Chuzhou with the respective finest grid size of 12 and 9 km, due likely to the later model initial times they used (i.e., 0800 and 1200 UTC 4 July), the rainfall amounts appear to be too excessive. Thus, our results indicate that increasing the grid spacing tends to underpredict the rainfall peaks and overpredict the coverage of heavy rainfall, with significant errors in position and timing. This result appears to differ from that obtained by some of the previous studies, which showed little added value as forecast guidance for heavy rainfall by decreasing the grid spacing from 4 to 2 km (e.g., Kain et al. 2008; Weisman et al. 2008; Schwartz et al. 2009). By comparing the three model runs, we may attribute the more realistic simulation of rainfall intensity and distribution, shown in Fig. 1a, to the use of the subkilometer grid spacing and the associated cloud microphysics, given the reasonable representation of the mei-yu front and meteorological fields upstream in the enhanced NCEP FNL analysis, and topography.

To further demonstrate the model's capability of reproducing the detailed heavy-rainfall structures from the large-scale initial conditions, we compare in Fig. 7 the time series of hourly rainfall at Chuzhou, located between the simulated maximum rainfall "station" (i.e., C at 32.4°N, 118.5°E, which is about 20 km to the northeast of Chuzhou) and the automatic rain gauge observations, together with the surface reports at Nanjing. The surface

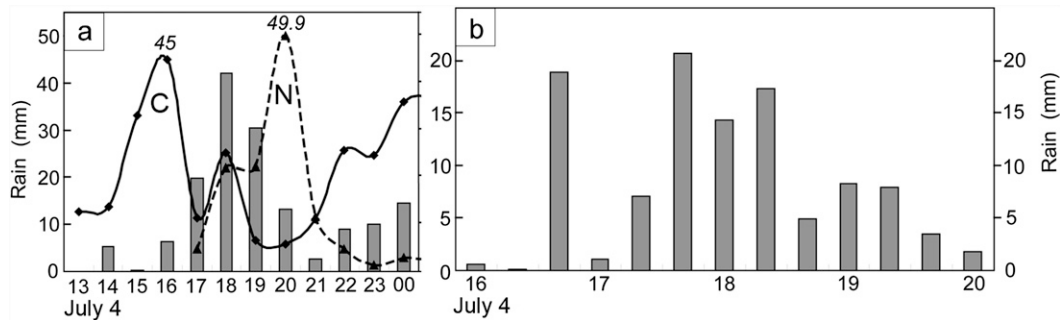


FIG. 7. Time series of (a) the observed hourly rainfall (mm) at Chuzhou (solid) and Nanjing (dashed) and the control-simulated 1-km area-averaged hourly rainfall at C (32.4°N, 118.5°E) from D4 (columns) during 1300 UTC 4 Jul–0000 UTC 5 Jul 2003. (b) The simulated 20-min rainfall (mm) at C (32.4°N, 118.5°E) during 1600–2000 UTC 4 Jul 2003.

reports show three rainfall centers hitting Chuzhou (i.e., at 1600 and 1800 UTC 4 July and 0000 UTC 5 July), but only one center at Nanjing (i.e., 2000 UTC 4 July), indicating pronounced spatial variability of rainfall within a distance of 50 km (Fig. 7a). The rainfall centers coincide well with the high cloud tops seen in satellite images (cf. Figs. 7a and 4). In contrast, the model produces two rainfall centers (i.e., 18 and 24 h into the integration), albeit occurring at different timings compared to the observed. Nevertheless, the simulated 20-min resolution map, given in Fig. 7b, does show the development of 3–4 rainfall centers during the 4-h period of 1600–2000 UTC 4 July, suggesting that the accumulated heavy rainfall at Chuzhou results from the passage of several convective elements within the MCS ahead of the mei-yu front. Such echo-training features are similar to those discussed by Doswell et al. (1996), Schumacher and Johnson (2008), Trier et al. (2006), and those simulated by Kato and Goda (2001). Clearly, only high-resolution simulations could capture such high-frequency rainfall scenarios and the associated convective elements, as indicated by comparing Figs. 7a and 7b.

Figure 8 shows that the vertically mass-weighted hydrometeors (i.e., the sum of cloud water, rainwater, ice, snow, and graupel) from the model simulation can be used to indicate the general distribution of rainfall. For example, the 18-h simulated total hydrometeors (shaded) exhibit a local maximum near Chuzhou, corresponding to the rainfall peak shown in Fig. 7a, and a few weaker centers upstream that appear to account for the passage of several rainfall peaks at Chuzhou and Nanjing at later times. This suggests that the modeled hydrometeors may be used as a useful variable to aid in the analysis and prediction of heavy rainfall in the future when such high-resolution NWP models can be run at an operational setting. Of course, this could be useful only after verifying against satellite, radar, or other types of observations.

Indeed, the general distribution of the simulated total hydrometeors compares favorably to satellite images (cf. Figs. 8 and 4c) despite the use of large-scale initial conditions. Mt. Dabie appears to help enhance convective development upstream and weaken it at the immediate downstream, as can also be seen from the observed rainfall (Fig. 1a).

Figure 9 compares the simulated radar reflectivity at 850 hPa, following Liu et al. (1997), to the observed at the radar site of Hefei at three selected times. Note that the 17-h simulated reflectivity data are used to verify against the observed values at 1600 UTC 4 July (cf. Figs. 9a,d), due partly to the slow model spinup and partly to the possible lacking small-scale details in the model initial conditions. Lean et al. (2008) have also noted such

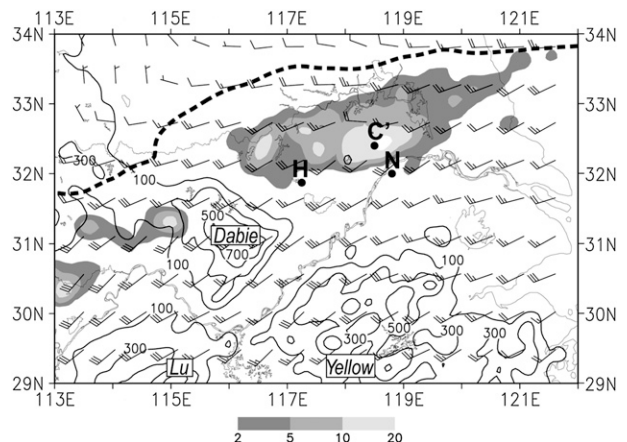


FIG. 8. Distribution of the vertically mass-weighted hydrometeors [i.e., the sum of cloud water, rainwater, cloud ice, snow, and graupel (unit: mm)], superposed with wind barbs (a full barb is 5 m s^{-1}) at 850 hPa, at the 18-h control simulation over D2. Topography at intervals of 200 m is also plotted, with Mt. Dabie, Mt. Lu, and Mt. Yellow indicated. Thick dashed lines denote the distribution of $\theta_e = 345 \text{ K}$ or the mei-yu front.

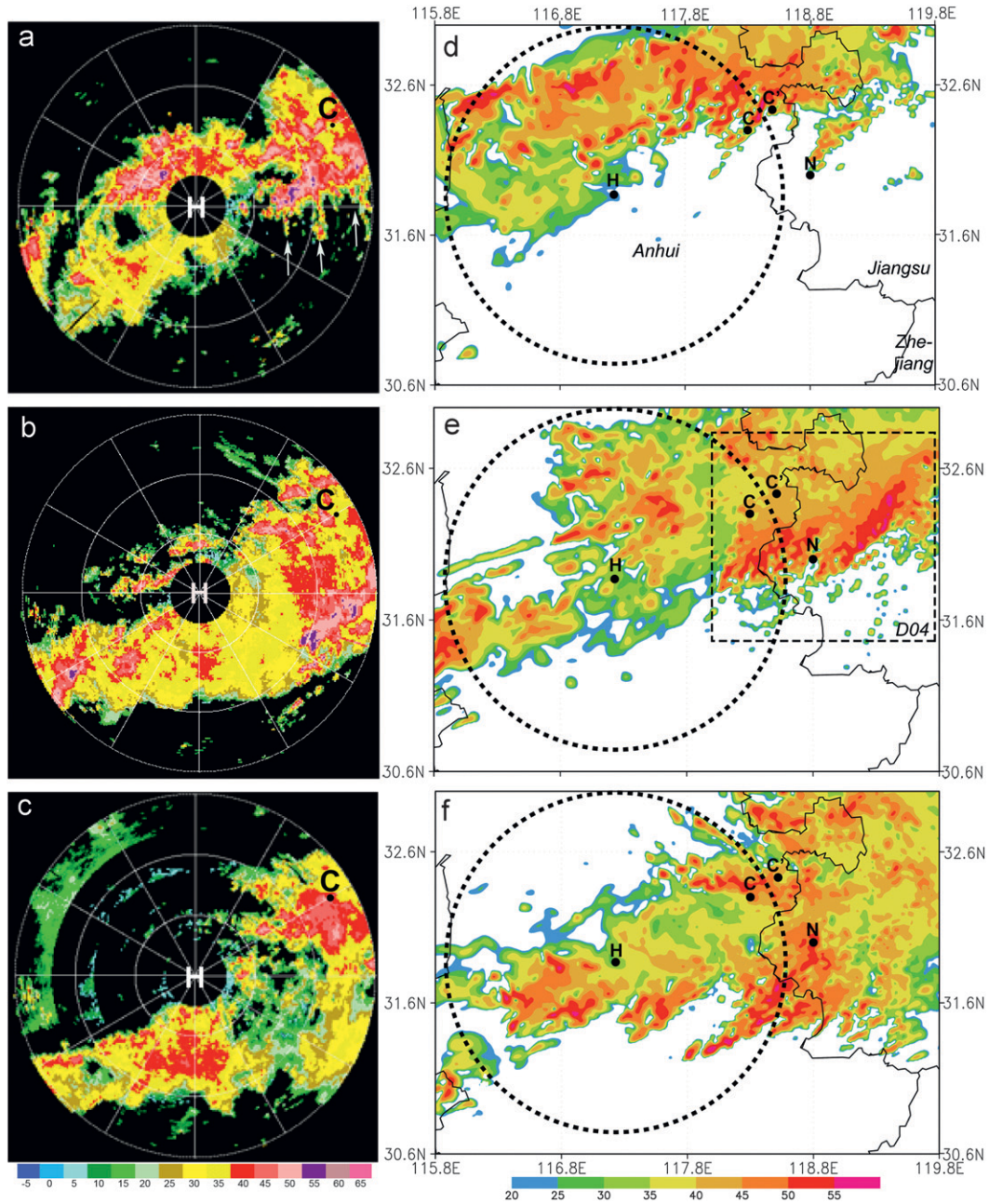


FIG. 9. Comparison of the radar reflectivity (dBZ) from Hefei's site at (a) 1600 and (b) 2000 UTC 4 Jul and (c) 0000 UTC 5 Jul 2003 to (d) 17-, (e) 20-, and (f) 24-h control-simulated reflectivity at 850 hPa over D3. Dotted lines in (d)–(f) show the maximum radial range (i.e., 150 km) of Hefei's radar, and the dashed frame in (e) denotes the portion of D4. Provincial borders of Anhui, Jiangsu, and Zhejiang are also plotted.

a model spinup problem during the first few hours integration as a finer grid mesh is activated from its mother grid mesh. Hefei's radar screen shows two northeast–southwest-oriented convective lines (cf. Figs. 9a and 4c): one narrow leading line associated with S_1 moving southeastward and one wide trailing line associated with S_2 moving eastward along and ahead of the mei-yu front.

At this time, the leading convective line just passed by Chuzhou with heavy rainfall (cf. Figs. 7a and 9a). Of interest is the development of many convective cells during the evening hours (Figs. 9a,b), some organized into the north–south-oriented convective bands, ahead of the leading convective line, as indicated by arrows in Fig. 9a. As will be seen in the next section, they result from the

lifting of the southwesterly high- θ_e air at the convectively generated cold outflow boundaries.

By 2000 UTC (Fig. 9b), the leading convective line developed into a more intense squall line, with several peak reflectivity spots of 55 dBZ (equivalent to a rainfall rate of about 100 mm h^{-1}), whereas the northeastern portion of the trailing convective line has weakened and become part of the trailing stratiform region [see Zhang et al. (2009) for a three-dimensional view]. On average, the southwest–northeast-oriented squall line moved *near-eastward* at a speed of about 10 m s^{-1} , but individual convective elements in the squall line and its trailing region moved *northeastward* at much faster speeds under the influence of larger-scale southwesterly flows. The squall line moved out of Hefei's radar range ($R = 150 \text{ km}$) shortly after, and produced heavy rainfall at Nanjing (Fig. 7a). While Chuzhou was located in the trailing stratiform region after 2000 UTC 4 July, it was hit by another large-sized convective cluster moving northeastward along the mei-yu front, producing more rainfall by 0000 UTC 5 July than that occurred earlier (Figs. 9c and 7a). The MCS and the convective storms (i.e., those associated with S_2 and S_3) to its west began to weaken when the second diurnal cycle started (not shown).

The MM5, with the subkilometer grid spacing, mimics reasonably well most of the above-mentioned convective-scale features. They include (i) the development of the leading squall line and the trailing convective bands or clusters ahead of the mei-yu front, with weak convection to the west of Hefei at the earlier stages (Fig. 9d); (ii) the continuous upstream initiation of deep convection to the southwest of the MCS, which is similar to the back-building mode described by Bluestein and Jain (1985) and simulated by Kato and Goda (2001), contributing to the rainfall center over western Anhui (cf. Figs. 1a and 9); (iii) the general weakening of deep convection as it moved northeastward to the rear of the squall line; and (iv) the initiation of new convective cells at the outflow boundaries that are organized into southwest–northeast-oriented convective bands in the inflow region to the south (Figs. 9d–f). In particular, the model also reproduces the passage of a few convective bands on the northwest of Chuzhou that are embedded in the trailing stratiform region (Figs. 9e,f), accounting for the final torrential-rainfall episode by the end of the simulation.

We must acknowledge that the above-mentioned features are reproduced with some timing and location errors, because of certain limitations with the model initial conditions and physics parameterizations. Despite these deficiencies, the model's capability of reproducing the total rainfall, the squall line, rainbands and several meso- β -scale details, is particularly encouraging, when considering that they are generated from large-scale initial conditions.

5. Convective initiation and organization

After obtaining a reasonably good simulation, it is desirable to examine some important unobserved features that contribute to the initiation of deep convection and its subsequent organization into a heavy-rain-producing MCS in the vicinity of Chuzhou, using the simulated data. For this purpose, Figs. 10a–d show the distribution of pressure (hPa), vertical motion (m s^{-1}), and horizontal winds on the potential temperature $\theta = 307\text{-K}$ surface over a large domain. The superposition of (vertically sheared) horizontal winds with the low-level isentropic surface would allow us to examine how isentropic lifting, as described by Raymond and Jiang (1990), of high- θ_e air in the PBL contributes to the initiation and organization of deep convection. Indeed, the low-level isentropic surfaces tilt upward from about 960 hPa at the leading outflow boundaries to 840 hPa ahead of the mei-yu front over a distance of 300–400 km following the south-southwesterly flows (Figs. 10a–d). The orientation and distribution of isobars coincide with those of convectively generated cold outflows from the dissipated MCS during the early evening hours, like those shown in Fig. 3. The model appears to capture the leading convective line, as indicated by the upward motion of greater than 0.2 m s^{-1} on the $\theta = 307\text{-K}$ surface, along the old boundaries characterized by a steep isentropic slope (cf. Figs. 4b and 10a). This indicates that the south-southwesterly high- θ_e air tends to ascend isentropically the elongated old cold dome, thereby providing a favorable lifting mechanism for the initiation and organization of deep convection ahead of the mei-yu front. Note that the evolution of this decaying MCS is simulated with the simultaneous use of parameterized convection and explicit cloud schemes over D1 and D2 during the first 12-h integration (not shown).

At 1300 UTC 4 July, the southwest–northeast-oriented mei-yu front is simulated between 32° and 34°N , which is about 100 km to the north of Chuzhou (Fig. 10a). While satellite observations showed the initiation of several convective storms (i.e., S_1 , S_2 , S_3) to the northwest of the leading convective line 1 h earlier (Fig. 4b), the model simulation exhibits 2–3 weak ascent regions along an elongated zone to the northwest of Chuzhou, which resemble to a certain degree the observed (S_1 , S_2 , S_3), albeit with a 1–2-h delay. This delay in the convective initiation, similar to that found by Lean et al. (2008), could be attributed to typical problems with the model spinup of gridbox saturation from the large-scale initial conditions and coarser-resolution fields, especially when considering that the finest grid of 444 m is activated at 12 h into the simulation.

It is of importance that the convective initiation (or gridbox saturation) occurs as the southwesterly high- θ_e

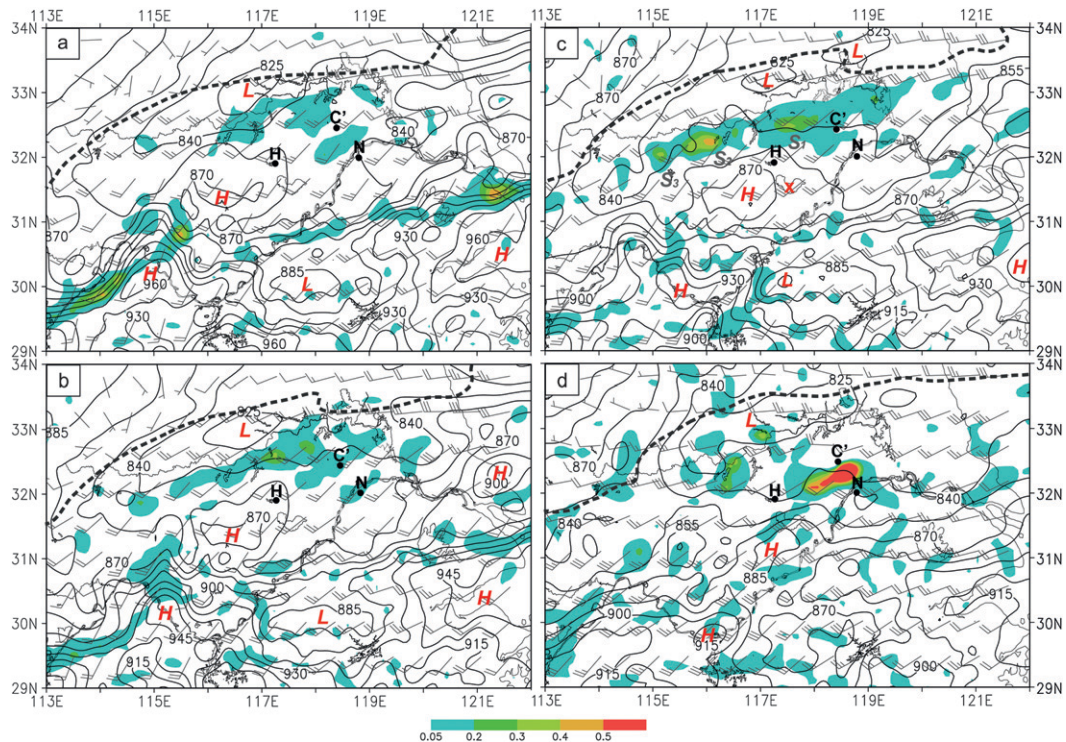


FIG. 10. Distribution of isobars (solid, every 15 hPa), and upward motion (m s^{-1} , colored), and horizontal wind bars on the $\theta = 307\text{-K}$ surface over a subdomain of D3 from (a) 13-, (b) 14-, (c) 15-, and (d) 18-h control simulations. The thick dashed lines in (a)–(d) show the location of the simulated mei-yu front, as denoted by $\theta_e = 345\text{ K}$ at 850 hPa. In (c), “x” denotes the sounding location shown in Fig. 12, and “S₁,” “S₂,” and “S₃” are used to indicate the three convective storms similar to those in Figs. 4b,c.

air ascends isentropically above the cold pool until reaching near the top of the bulged $\theta = 307\text{-K}$ surface, where the isentropic surface becomes more horizontal and flow convergence takes place as the (divergent) cold air below subsides. This lifting mechanism, like a “warm front,” and subsequent convective evolution appear to differ from those occurring at the leading edge of the old boundaries where the sloping isentropic surface is steep, which behaves like a “cold front.” More specifically, the leading edge convective triggering involves more the interaction of vertical wind shear and cold pool, as described by Rotunno et al. (1988) and Weisman and Rotunno (2004), whereas the above-mentioned three convective storms are triggered at about 200 km to the north of the leading edge where the vertical shear–cold pool dynamics appears to be less relevant. Given the cold pool intensity and distribution, the southwesterly moisture content would play an important role in determining when and where latent heat release may occur. In the present case, deep convection could be continuously triggered along the elongated, quasi-stationary convergence zone that is located about 100 km ahead of the mei-yu front, and then moves along the cold dome repeatedly across the

Hefei–Chuzhou region under the influence of southwesterly flows, leading to the heavy rainfall near Chuzhou as shown in Figs. 7 and 9. In fact, the convergence zone, coinciding roughly with the contour of $p = 840\text{-hPa}$ isobar, changes little in location and orientation during the 6-h evening period of 1200–1800 UTC 4 July, while the leading old cold outflow boundaries weaken as they move into the nocturnal stable boundary layer ahead.

By 1500 UTC 4 July, we see the development of three distinct convective storms (also labeled as S₁, S₂, and S₃) that are similar to those observed along a southwest–northeast-oriented convective line (cf. Figs. 10b,c and 4b,c). Its leading portion (i.e., S₁) has passed the city of Chuzhou, as could also be seen from Fig. 4c, and later it grows to a squall line as shown in Fig. 9d. The southward displacement of the 840-hPa isobar toward Chuzhou indicates the strengthening of the cold air mass by individual eastward-propagating convective storms (cf. Figs. 10b–d). West–east vertical cross sections along 29°N (i.e., about 350 km upstream from Chuzhou), given in Fig. 11, show the presence of an LLJ with the peak southwesterly wind speed increasing from 10 to 14 m s^{-1} near 900 hPa during the late evening hours, and an elevated layer between

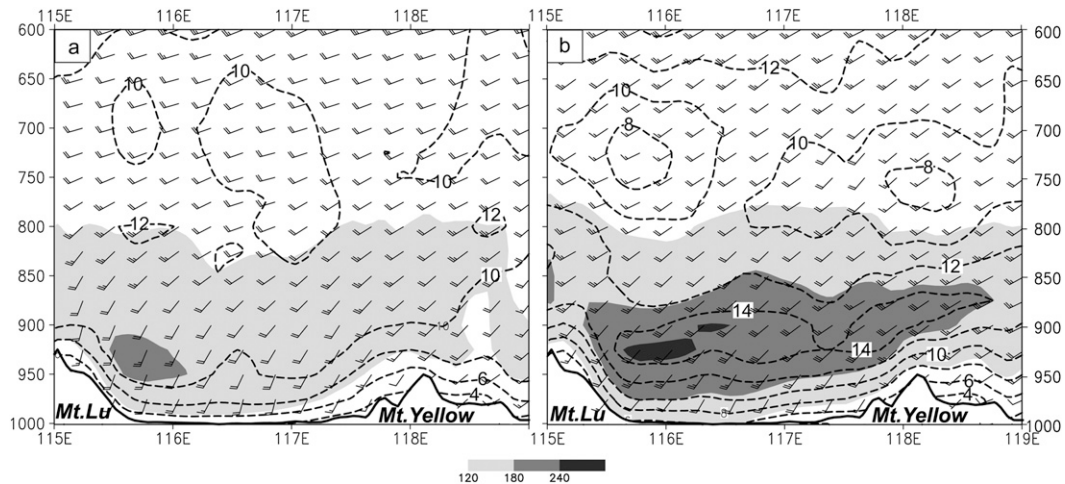


FIG. 11. West-east vertical cross sections of the moisture flux, $|\mathbf{V}|q_v$, [shadings, m g (kg s)^{-1}], where \mathbf{V} is the horizontal wind vector and q_v is the mixing ratio of water vapor, horizontal wind bars (a full barb is 5 m s^{-1}) and wind speed (dashed, every 2 m s^{-1}) up to 600 hPa along the latitude of 29°N from (a) 12- and (b) 18-h control simulations over D1. Mt. Lu and Mt. Yellow are also shown (see Fig. 8 for their distribution).

950 and 850 hPa of high moisture flux [$>200 \text{ m g (kg s)}^{-1}$] air within a width of at least 300 km. The sloping terrain of Mt. Lu, though only 700–800 m high, could contribute partly to the generation of the LLJ, as shown by a theoretical study by Holton (1967) and a model sensitivity study by D.-L. Zhang et al. (2006). Clearly, this northeastward moist supply helps maintain conditional instability and accounts for deep convection in the Chuzhou–Nanjing area, which is similar to that described by Trier et al. (2006). Note that the mesoscale moist air current displaces eastward as does the heavy-rain-producing MCS, thus providing necessary CAPE for convective development as it isentropically ascends the underlying cold dome.

Figure 12 shows a sounding, taken from the 15-h simulation at about 100 km southwest of Chuzhou and 250 km to the north of the cross section given in Fig. 11, shows a thermal inversion (i.e., associated with the old cold pool) in the bottom 40 hPa, an isentropic-ascending shallow warm air layer between 900 and 960 hPa, a moist layer (associated with the southwesterly monsoonal air) from 900 to 700 hPa, and a dry layer aloft. Although this sounding reveals the presence of local weak convective inhibition in the lowest 150 hPa, considerable CAPE (as high as 1930 J kg^{-1}) can be available once the isentropic-ascending warm and moist air reaches the LCL. It follows that the continued strengthening of the southwesterly LLJ would feed necessary CAPE for convective development in the vicinity of Chuzhou and Nanjing during the evening hours. It also accounts for the southeastward advancement of deep convection as a result of the interaction of (vertical sheared) moist monsoonal air with convectively generated cold outflows (Rotunno et al. 1988; Weisman

and Rotunno 2004), until the early morning hours of 5 July (Figs. 9d–f).

Figure 13 shows the meso- β -scale structures and evolution of precipitation, and convectively generated perturbations of surface pressure, temperature, and horizontal winds associated with the heavy-rain-producing MCS. These surface perturbations are more pronounced about 5 h into the integration of D4 (i.e., starting 1700 UTC 4 July). At this time, several southwest–northeast-oriented

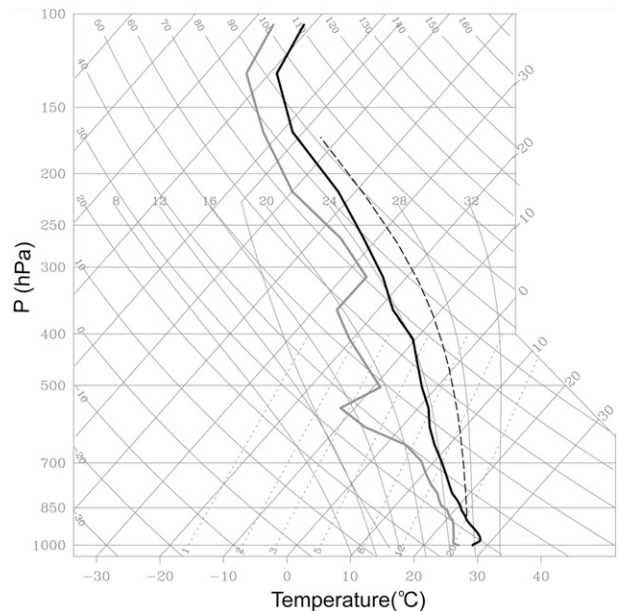


FIG. 12. A skew T -log p plot taken at 31.5°N , 117.5°E (i.e., at point “ \times ” in Fig. 10c) from the 15-h simulation over D1.

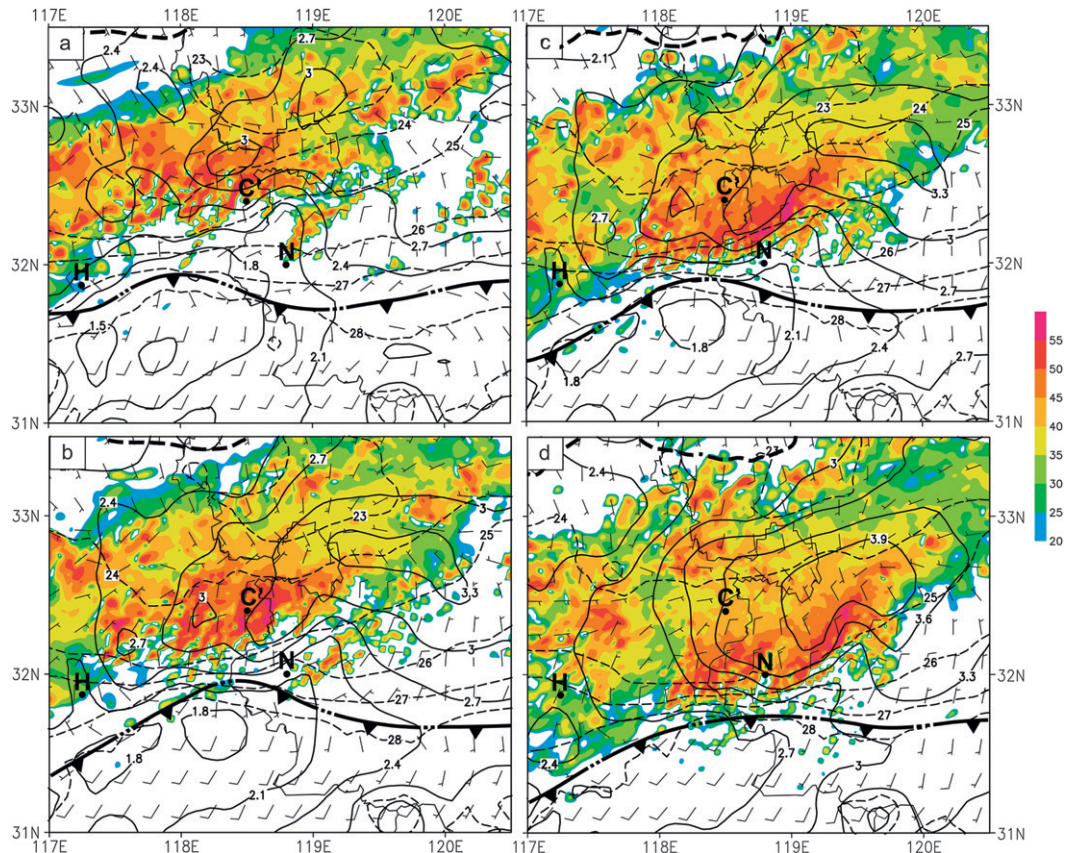


FIG. 13. Analyses of the sea level pressure (solid, every 0.3 hPa in excess of 1000 hPa), radar reflectivity (shadings), surface temperature (dashed, every 1°C), and surface winds (a full barb is 5 m s^{-1}) over a subdomain of D3 from (a) 17-, (b) 18-, (c) 19-, and (d) 20-h control simulations. Thick dashed lines denote the distribution of $\theta_e = 345\text{ K}$ or the mei-yu front.

convective rainbands with a length scale of 20–50 km take place in the vicinity of Chuzhou, as also shown in Figs. 9d–f. It is the passage of these rainbands (i.e., echo training) that causes the heavy rainfall at Chuzhou. A well-developed meso-high pressure center is located on the immediate northeastern side of the squall line (i.e., in the stratiform region between the mei-yu front and Chuzhou), with widespread cold outflows nearly 90° across local isobars (Fig. 13a). This indicates the important roles of evaporative cooling, likely initiated in the midlevel minimum θ_e layer, from discrete convective cells, in continuously building up the cold pool beneath. Ahead of the squall line is a weak presquall trough to the south, and a mesotrough farther to the south associated with the previously dissipated MCS, as indicated by frontal symbols. These convectively driven surface perturbations have been found in the surface analyses of MCSs by Maddox et al. (1980), Johnson and Hamilton (1988), and Fritsch et al. (1994), and simulated by Zhang and Fritsch (1986), and Zhang et al. (1989), using much coarser resolution models with parameterized convection. However, there

is little evidence of wake pressure lows, as shown in Johnson and Hamilton (1988), and Zhang et al. (1989), in the present case, indicating the likely absence of mesoscale dry rear-to-front descending flows (Houze et al. 1989; Zhang and Gao 1989).

Note that although southerly surface inflows converge with cold outflows along the mesotrough, few convective cells could be triggered along the leading old outflow boundaries, due partly to the presence of a stable layer in the lowest layer (Fig. 12), and partly to the lack of enough lifting to the LCL. Organized deep convection occurs at some distance behind the leading outflow boundaries. It should be mentioned that the larger-scale organization, as shown in Figs. 2, 3, and 13, is to some extent similar to that of the meso-high type of flash flood events occurring often nocturnally in the United States (Maddox et al. 1979; Schumacher and Johnson 2005), except for the important roles of the mei-yu front. Perhaps an important difference from the meso-high conceptual model is the echo training process that occurs from northwest in the wake of the leading convective line (Figs. 9 and 13),

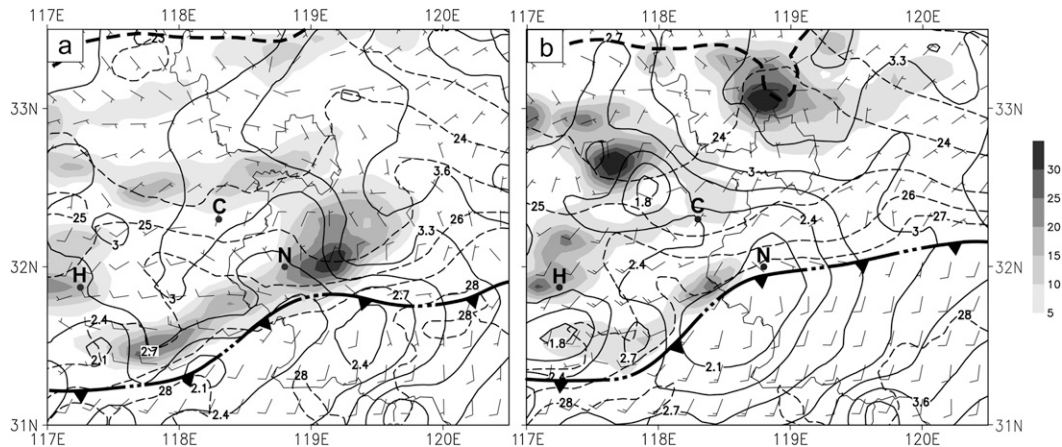


FIG. 14. As in Fig. 13d, but for the hourly rainfall rate (shadings) at the ground from (a) 1.33 km (i.e., the nested 12/4/1.33-km run) and (b) 4 km (i.e., the nested 12/4-km run).

rather than from southwest beginning at the leading line (Maddox et al. 1979).

The surface pressure structures are closer to those of meso-high-type events at 1800 UTC 4 July, when heavy rainfall has begun near Chuzhou (cf. Figs. 13b and 7a). That is, a local meso-high forms behind the southeastward-moving squall line with the presquall trough better developed, while the cold air mass to the north keeps moving eastward along the mei-yu front, as indicated by another meso-high center in the far stratiform region to the northeast (cf. Figs. 13b and 9d,e). After passing the city of Nanjing, the squall line begins to weaken with reduced rainfall (Figs. 13c,d). The model simulation indicates that the lack of lifting and the reduced LLJ strength (and moisture flux) are responsible for the weakening of the storm (not shown). Of significance is that the MCS leaves behind a large-sized meso-high pressure system over the region (Fig. 13d), as a result of considerable evaporation associated with midlevel dry intrusion (Figs. 5 and 12).

Finally, Figs. 14a,b show the same surface fields at 2000 UTC 4 July as those shown in Fig. 13d, except for the surface hourly rainfall rate from the nested 1.33- and 4-km runs, respectively. The simulated reflectivity field from the two sensitivity runs is not shown because the intensities of vertical motion and precipitation are sensitive to grid resolution, and because the 4-km run includes the Kain–Fritsch convective scheme. Nevertheless, the 1.33-km run shows much less detailed rainfall. In addition, the leading convective line moves too fast prior to the 20-h control simulation and slow afterward, causing less and more rainfall in the wake region and leading edge, respectively (cf. Figs. 14a and 13d and 1b,a). The simulated surface pressure perturbations and outflows are also much weaker than those in the control run. Increasing the finest

grid spacing to 4 km fails to reproduce the generation and movement of the intense squall line as well as the surface meso-high and its associated outflows (cf. Figs. 14b and 13d), due to the lack of convectively generated moist downdrafts by both the Kain–Fritsch convective scheme and the Tao–Simpson cloud microphysics scheme. Instead, the model produces several localized storms, one of which induces a mesolow with pronounced convergence and rotation to the northwest of Chuzhou.

A comparison of Figs. 13d and 14a,b suggests that the absence of an intense meso-high or cold dome accounts for the less realistically organized convection and rainfall fields in both sensitivity simulations. When the finest 12-km grid spacing is used (M. Zhang et al. 2006), the model produces a considerable amount of grid-scale rainfall, causing the formation of a larger surface mesolow over east China (not shown), which is similar to CISK-like instability described by Zhang et al. (1988), Molinari and Dudek (1992), and Zhang et al. (1994). Similarly, with the use of convective parameterizations, Liao and Tan (2005) and Wang and Ni (2006) also produced excessive rainfall and a low-level mesolow or mesovortex associated with the torrential-rain-producing storm in their 12- and 9-km grid-spacing simulations, respectively. Similar results were also shown by Liu et al. (2010) in the regional climate simulations of the summer 1998 extreme rainfall in east China using even the finest grid size of 4 km.

6. Summary and conclusions

In this study, we examined the development of exceptional torrential rainfall in the vicinity of Chuzhou, east China, during the evening hours of 4–5 July 2003 using the NCEP FNL analysis, mesoscale surface analysis, rain gauge, satellite and radar data, and a 24-h (MM5)

nested-grid simulation with the finest grid size of 444 m. To our knowledge, this appears to be the first real-data case simulation with such a fine resolution to examine the multiscale characteristics of torrential-rainfall events, and the potential improvements of QPFs and their mesoscale circulations, associated with the mei-yu front and MCSs.

Observational analyses show that east China on 4–5 July was dominated by a favorable large-scale environment with moderate cold advection aloft and the southwesterly transport of high- θ_e or moist monsoonal air below, toward the mei-yu front, and cold outflow boundaries left behind a dissipating MCS during the daytime of 4 July. Satellite images and rain gauges indicate the initiation of three convective storms between the old boundaries and mei-yu front on the west of Chuzhou during the early evening hours, the development of an intense MCS with torrential rainfall at Chuzhou near midnight, and the dissipation of the MCS shortly after 0000 UTC 5 July.

Verification of the subkilometer simulation with available observations shows encouraging skill of the MM5 in reproducing the distribution and magnitude of the observed rainfall, especially the torrential amount at nearly the right location, albeit with a 1–2-h delay and about 100 mm less rainfall. In particular, the model reproduces the evolution of the dissipating MCS and its associated cold outflows mostly on the intermediate 1.33-km grid mesh, the triggering of several separate convective storms (i.e., backbuilding) near the top of the southwest–northeast-elongated old cold dome ahead of the mei-yu front, the subsequent organization into a large MCS, and the generation of an intense meso-high associated with a convectively enhanced cold dome, meso- β -scale radar reflectivity morphologies, and the passage of several heavy-rain-producing convective bands near Chuzhou at the leading convective line and in the trailing stratiform region. It is shown that the above features are poorly simulated, especially the peak rainfall and surface circulations, when the finest 1.33- and 4-km grid configurations are used.

Results from the subkilometer simulation indicate that (i) the isentropic lifting of the (vertical sheared) moist monsoonal air over the cold dome ahead of the mei-yu front plays an important role in triggering the three earlier convective storms; (ii) convectively enhanced cold outflows, interacting with the (vertical sheared) moist environmental flows, assist in the subsequent organization and propagation of the MCS ahead of the mei-yu front; (iii) the development of a nocturnal southwesterly low-level jet provides necessary CAPE and moisture content for heavy-rainfall production; and (iv) the repeated upstream formation of convective cells over the elongated cold dome and their subsequent propagation along the same path (i.e., echo training) cause the torrential rainfall over the Chuzhou–Nanjing region. Results also show

that the torrential-rainfall generation is similar to the meso-high type of flash flood events often occurring nocturnally in the United States, except for the echo training process that occurs in the wake of the leading convective line.

Recognizing that a single case study could not provide a rigorous test of the predictability of multiscale characteristics of torrential-rainfall events with a subkilometer cloud-resolving model, the results indicate that it may be possible to improve summertime QPFs associated with the mei-yu fronts or other midlatitude MCSs, if high-resolution observations and realistic NWP models are used. Ideally, some well-designed ensemble simulations may have to be undertaken to address the predictability-related issues, which is beyond the scope of the present study. Nevertheless, the use of subkilometer NWP models may help reproduce more realistically localized extreme rainfall events and convectively generated meso- β -scale circulations than those models using convective parameterizations even at the finest grid size of 4 km.

In Part II of this series of papers, the subkilometer model simulation will be diagnosed to investigate the meso- β - and γ -scale circulation structures along the leading convective line, the interaction of cold outflows with the environmental vertical wind shear and CAPE in initiating new convection along the leading line and in the wake region and determining the orientation of the leading convective line, and the local water budget associated with the torrential-rainfall events.

Acknowledgments. We wish to thank Prof. Y. Ni for providing the field observations used for the present study and Dr. Russ Schumacher and two anonymous reviewers for their constructive comments. This work was supported by NSFC Grant 40775060 and NSF Grant ATM0758609.

REFERENCES

- Bluestein, H. B., and M. H. Jain, 1985: Formation of mesoscale lines of precipitation: Severe squall lines in Oklahoma during the spring. *J. Atmos. Sci.*, **42**, 1711–1732.
- Bosart, L. F., and F. Sanders, 1981: The Johnstown flood of July 1977: A long-lived convective system. *J. Atmos. Sci.*, **38**, 1616–1642.
- Bryan, G. H., J. C. Wyngaard, and J. M. Fritsch, 2003: Resolution requirements for the simulation of deep moist convection. *Mon. Wea. Rev.*, **131**, 2394–2416.
- Caracena, F., R. A. Maddox, L. R. Hoxit, and C. F. Chappell, 1979: Mesoanalysis of the Big Thompson storm. *Mon. Wea. Rev.*, **107**, 1–17.
- Chen, G. T.-J., and C. C. Yu, 1988: Study of low-level jet and extremely heavy rainfall over northern Taiwan in the mei-yu season. *Mon. Wea. Rev.*, **116**, 884–891.
- Chen, S.-J., Y.-H. Kuo, W. Wang, Z.-Y. Tao, and B. Cui, 1998: A modeling case study of heavy rainstorms along the mei-yu front. *Mon. Wea. Rev.*, **126**, 2330–2351.

- Clark, A. J., W. A. Gallus Jr., M. Xue, and F. Kong, 2009: A comparison of precipitation forecast skill between small convection-allowing and large convection-parameterizing ensembles. *Wea. Forecasting*, **24**, 1121–1140.
- Ding, Y.-H., and J. C. L. Chan, 2005: The East Asian summer monsoon: An overview. *Meteor. Atmos. Phys.*, **89**, 117–142.
- Doswell, C. A., III, H. E. Brooks, and R. A. Maddox, 1996: Flash flood forecasting: An ingredients-based methodology. *Wea. Forecasting*, **11**, 560–581.
- Dudhia, J., 1989: Numerical study of convection observed during the Winter Monsoon Experiment using a mesoscale two-dimensional model. *J. Atmos. Sci.*, **46**, 3077–3107.
- , 1993: A nonhydrostatic version of the Penn State–NCAR mesoscale model: Validation tests and simulation of an Atlantic cyclone and cold front. *Mon. Wea. Rev.*, **121**, 1493–1513.
- Fritsch, J. M., J. D. Murphy, and J. S. Kain, 1994: Warm core vortex amplification over land. *J. Atmos. Sci.*, **51**, 1780–1807.
- , and Coauthors, 1998: Quantitative precipitation forecasting: Report of the Eighth Prospectus Development Team, U.S. Weather Research Program. *Bull. Amer. Meteor. Soc.*, **79**, 285–299.
- Grell, G. A., J. Dudhia, and D. R. Stauffer, 1995: A description of the fifth-generation Penn State/NCAR mesoscale model (MM5). NCAR Tech Note NCAR/TN-398+STR, 138 pp. [Available from NCAR Publication Office, P.O. Box 3000, Boulder, CO 80307-3000.]
- Holton, J. R., 1967: The diurnal boundary layer wind oscillation above sloping terrain. *Tellus*, **19**, 199–205.
- Houze, R. A., Jr., S. A. Rutledge, M. I. Biggerstaff, and B. F. Smull, 1989: Interpretation of Doppler weather-radar displays in midlatitude mesoscale convective systems. *Bull. Amer. Meteor. Soc.*, **70**, 608–619.
- Johnson, R. H., and P. J. Hamilton, 1988: The relationship of surface pressure features to precipitation and airflow structure of an intense midlatitude squall line. *Mon. Wea. Rev.*, **116**, 1444–1472.
- Kain, J. S., 2004: The Kain–Fritsch convective parameterization: An update. *J. Appl. Meteor.*, **43**, 170–181.
- , and Coauthors, 2008: Some practical considerations regarding horizontal resolution in the first generation of operational convection-allowing NWP. *Wea. Forecasting*, **23**, 931–952.
- Kato, T., 2006: Structure of the band-shaped precipitation system inducing the heavy rainfall observed over northern Kyushu, Japan on 29 June 1999. *J. Meteor. Soc. Japan*, **84**, 129–153.
- , and H. Goda, 2001: Formation and maintenance processes of a stationary band-shaped heavy rainfall observed in Niigata on 4 August 1998. *J. Meteor. Soc. Japan*, **79**, 899–924.
- Lean, H. W., P. A. Clark, M. Dixon, N. M. Roberts, A. Fitch, R. Forbes, and C. Halliwell, 2008: Characteristics of high-resolution versions of the Met Office Unified Model for forecasting convection over the United Kingdom. *Mon. Wea. Rev.*, **136**, 3408–3424.
- Liao, J., and Z. Tan, 2005: Numerical simulation of a heavy rainfall event along the Meiyu front: Influences of different scale weather systems (in Chinese). *Acta Meteor. Sin.*, **63**, 771–789.
- Liu, H., D.-L. Zhang, and B. Wang, 2010: Impact of horizontal resolution on the regional climate simulations of the Summer 1998 extreme rainfall along the Yangtze-River Basin. *J. Geophys. Res.*, **115**, D12115, doi:10.1029/2009JD012746.
- Liu, Y., D.-L. Zhang, and M. K. Yau, 1997: A multiscale numerical study of Hurricane Andrew (1992). Part I: Explicit simulation and verification. *Mon. Wea. Rev.*, **125**, 3073–3093.
- Maddox, R. A., C. F. Chappell, and L. R. Hoxit, 1979: Synoptic and meso- α -scale aspects of flash flood events. *Bull. Amer. Meteor. Soc.*, **60**, 115–123.
- , F. Canova, and L. R. Hoxit, 1980: Meteorological characteristics of flash flood events over the western United States. *Mon. Wea. Rev.*, **108**, 1866–1877.
- Molinari, J., and M. Dudek, 1992: Parameterization of convective precipitation in mesoscale numerical models: A critical review. *Mon. Wea. Rev.*, **120**, 326–344.
- Qian, J.-H., W.-K. Tao, and K.-M. Lau, 2004: Mechanisms for torrential rain associated with the mei-yu development during SCSMEX 1998. *Mon. Wea. Rev.*, **132**, 3–27.
- Raymond, D. J., and H. Jiang, 1990: A theory of long-lived mesoscale convective systems. *J. Atmos. Sci.*, **47**, 3067–3077.
- Rotunno, R., J. B. Klemp, and M. L. Weisman, 1988: A theory for strong, long-lived squall lines. *J. Atmos. Sci.*, **45**, 463–485.
- Schumacher, R. S., and R. H. Johnson, 2005: Organization and environmental properties of extreme-rain-producing mesoscale convective systems. *Mon. Wea. Rev.*, **133**, 961–976.
- , and —, 2008: Mesoscale processes contributing to extreme rainfall in a midlatitude warm-season flash flood. *Mon. Wea. Rev.*, **136**, 3964–3986.
- , and —, 2009: Quasi-stationary, extreme-rain-producing convective systems associated with midlevel cyclonic circulations. *Wea. Forecasting*, **24**, 555–574.
- Schwartz, C. S., and Coauthors, 2009: Next-day convection-allowing WRF model guidance: A second look at 2-km versus 4-km grid spacing. *Mon. Wea. Rev.*, **137**, 3351–3372.
- Stauffer, D. R., and N. L. Seaman, 1990: Use of four-dimensional data assimilation in a limited-area mesoscale model. Part I: Experiments with synoptic-scale data. *Mon. Wea. Rev.*, **118**, 1250–1277.
- Sun, J.-H., H.-G. Zhou, and S.-X. Zhao, 2006: An observational study of mesoscale convective systems producing severe heavy rainfall in the Huaihe River Basin during 3–4 July 2003 (in Chinese). *Chin. J. Atmos. Sci.*, **30**, 1103–1118.
- Tao, W.-K., and J. Simpson, 1993: The Goddard cumulus ensemble model. Part I: Model description. *Terr. Atmos. Ocean Sci.*, **4**, 35–72.
- Trier, S. B., C. A. Davis, D. A. Ahijevych, M. L. Weisman, and G. H. Bryan, 2006: Mechanisms supporting long-lived episodes of propagating nocturnal convection within a 7-day WRF model simulation. *J. Atmos. Sci.*, **63**, 2437–2461.
- Wang, H., and Y. Ni, 2006: Diagnostic analysis and numerical simulation of a mesoscale torrential rainsystem in the Huaihe valley during the rainy season in 2003 (in Chinese). *Acta Meteor. Sin.*, **64**, 734–742.
- Weisman, M. L., and R. Rotunno, 2004: “A theory for strong long-lived squall lines” revisited. *J. Atmos. Sci.*, **61**, 361–382.
- , C. Davis, W. Wang, K. W. Manning, and J. B. Klemp, 2008: Experiences with 0–36-h explicit convective forecasts with the WRF-ARW model. *Wea. Forecasting*, **23**, 407–437.
- Zhang, D.-L., and R. A. Anthes, 1982: A high-resolution model of the planetary boundary layer—Sensitivity tests and comparisons with SESAME-79 data. *J. Appl. Meteor.*, **21**, 1594–1609.
- , and J. M. Fritsch, 1986: Numerical simulation of the meso- β -scale structure and evolution of the 1977 Johnstown flood. Part I: Model description and verification. *J. Atmos. Sci.*, **43**, 1913–1943.
- , and K. Gao, 1989: Numerical simulation of an intense squall line during 10–11 June 1985 PRE-STORM. Part II: Rear inflow, surface pressure perturbations, and stratiform precipitation. *Mon. Wea. Rev.*, **117**, 2067–2094.

- , H.-R. Chang, N. L. Seaman, T. T. Warner, and J. M. Fritsch, 1986: A two-way interactive nesting procedure with variable terrain resolution. *Mon. Wea. Rev.*, **114**, 1330–1339.
- , E.-Y. Hsie, and M. W. Moncrieff, 1988: A comparison of explicit and implicit predictions of convective and stratiform precipitating weather systems with a meso- β -scale numerical model. *Quart. J. Roy. Meteor. Soc.*, **114**, 31–60.
- , K. Gao, and D.-B. Parsons, 1989: Numerical simulation of an intense squall line during 10–11 June 1985 PRE-STORM. Part I: Model verification. *Mon. Wea. Rev.*, **117**, 960–994.
- , J. S. Kain, J. M. Fritsch, and K. Gao, 1994: Comments on “Parameterization of convective precipitation in mesoscale numerical models: A critical review.” *Mon. Wea. Rev.*, **122**, 2222–2231.
- , S. Zhang, and S. Weaver, 2006: Low-level jets over the mid-Atlantic states: Warm-season climatology and a case study. *J. Appl. Meteor. Climatol.*, **45**, 194–209.
- Zhang, M., A. S. Wang, Z. Z. Ji, and W. L. Zhang, 2006: Influence of different precipitation parameterization schemes on a simulated “03.7” heavy rainfall case (in Chinese). *Chin. J. Atmos. Sci.*, **30**, 441–452.
- , D.-L. Zhang, and A. Wang, 2009: Numerical simulation of torrential rainfall and vortical hot towers in a midlatitude mesoscale convective system. *Atmos. Oceanic Sci. Lett.*, **2**, 188–192.